electronics

MDPI

Article

Dynamic Modulation Band Rejection Filter Based on Spoof Surface Plasmon Polaritons

Weigao Yang [1,2], Lixiang Liu [2], Xiaoqiang Su [2], Lijuan Dong [2], Yanhong Liu [2] and Zhanfeng Li [1,3,*]

1 College of Physics and Optoelectronics, Taiyuan University of Technology, Taiyuan 030024, China; weigyang@163.com
2 Shanxi Provincial Key Laboratory of Microstructure Electromagnetic Functional Materials, Shanxi Datong University, Datong 037009, China; liulx_2002@163.com (L.L.); xqsu615@gmail.com (X.S.); Donglijuan_2012@163.com (L.D.); Lyh030114@163.com (Y.L.)
3 Key Laboratory of Advanced Transducers and Intelligent Control System, Ministry of Education and Shanxi Province, Taiyuan University of Technology, Taiyuan 03002, China
* Correspondence: lizhanfeng@tyut.edu.cn

Received: 3 May 2020; Accepted: 10 June 2020; Published: 13 June 2020

Abstract: In this paper, we proposed a dynamic modulation band rejection filter based on the spoof surface plasmon polaritons (SSPPs) waveguide. The dynamic adjusting mainly derives from changing the capacitance between the U-shape and the waveguide configuration. The capacitance can modulate the cut-off frequency of fundamental mode. The rejection band is formed by the high order propagation mode and the cut-off frequency of fundamental mode. We analyzed the dispersion curve and transmission performance of the band rejection filter with different capacitances. Compared with the previous scheme, the design we proposed here has a simpler and more delicate configuration to process and decreases the mechanical error. We experimentally demonstrated the excellent performance of the device by changing the direct voltage loaded on the varactor diode and achieved real time modulation around 2 GHz.

Keywords: spoof surface plasmon polaritons; filter; dynamic modulation

1. Introduction

As a kind of special surface wave, surface plasmon polaritons (SPPs) exist at the interface of metal and dielectric, which propagate along the interface and attenuate exponentially in the direction of normal interface [1–3]. At high frequency electromagnetic range, SPPs can be excited naturally because the metal behaves as plasma, with negative permittivity. It had been proven that the SPPs have the ability to confine and enhance the near electromagnetic field, so they will bring a lot of innovative technologies and applications, such as subwavelength focusing [4–6], subwavelength imaging [4,5,7], biosensing [8–11], harmonics generation [12,13], photonic integrated circuit and waveguide [6,14–17]. At a lower frequency, for example, the microwave and terahertz frequency range, SPPs cannot exist because the metal behaves like the perfect electrical conductor (PEC), rather than the plasma with negative permittivity. By means of metamaterial, the so-called spoof SPPs (SSPPs) or designer SPPs have been proposed, which can also produce a highly localized surface wave and inherit other properties at the high frequency [18,19]. The metal surface, decorated with a one-dimensional array of groove, two-dimensional wedges and holes, can excite the SSPPs [16,20,21]. Furthermore, the dispersion and field confinement of SSPPs can be designed and controlled by changing the geometrical parameters of the unit cell. However, most traditional waveguide devices are made of three-dimensional (3D) structures, which are complicated to produce and difficult to integrate with microwave circuits.

To apply SSPPs devices in practice, conformal surface plasmon constructions on planar flexible films have been proposed, which can propagate the spoof SPPs in the form of a bent and spiral shape [22]. Therefore, it is a promising solution for spoof SPPs to apply in future microwave integrated circuit regions [23].

Some functional devices based on SSPPs have been proposed in the last few years [24–26]. However, traditional devices based on SSPPsconsist of a passive unit, such as waveguide formed by patch [21], which lacks dynamic modulation. Considering that the function of a passive device is fixed once the dimension and configuration confirmed, the devices which can be dynamically modulated are required in modern microwave systems. Recently, many interesting works about active devices have been reported, for example, in microwave frequency, programmable plasmonic devices [27–29], tunable power dividers [30], reconfigurable metalenses [31,32], polarization converters [33] and other reconfigurable devices [34–38]. Tracing previous researchers' thoughts [27,35,36], here we proposed an active modulation band rejection filter through controlling the cut-off frequency between the fundamental mode and the high order mode, which arises from changing capacitance generated between the waveguide and U-shape ring. The filter we present here has a simpler configuration that makes the sample easier to produce and decreases the mechanical error to some extent, compared with the former design [27].

2. SSPPs Waveguide Design

In this work, we proposed an active filter based on spoof SPPs waveguide in the microwave frequency. A single layer F4B is selected as the substrate, whose thickness is 0.508 mm with the relative dielectric constant and loss tangent at 2.56 and 0.001. Annealed copper (with electric conductivity σ = 5.8e + 007 S/m) is printed on the substrate and the metal with a thickness of 0.018 mm. The details of the proposed waveguide unit cell are plotted in Figure 1a, where p = 5.3 mm, h = 2 mm, wa = 0.2 mm, px = 3.5 mm, w2 = 3.5 mm, w3 = 0.5 mm and l4 = 1.6 mm. As demonstrated in ref [21], when decreasing the height of the patch, the dispersion curve gradually deviated from the light line, which proved that the configuration would decrease the speed of the electromagnetic wave and transform the conventional guided wave to spoof SPPs, smoothly. The dispersion curve of the unit cell is simulated by means of the Eigenmode solver of the commercial software CST Microwave Studio. In simulation, periodic boundaries are set along x direction, while the other directions are set to PEC boundaries, 50 mm away from the unit. The corresponding dispersion curve of the waveguide unit cell is shown in Figure 1b. From this figure, we can clearly see that the dispersion curves are blowing and deviating gradually from the light line and finally reach different cut-off frequencies. Furthermore, with decreasing the height of unit w2, the cut-off frequency increases correspondingly, which demonstrated that the geometric parameters can be used to design the dispersion characteristics of spoof SPPs. Hence, we gradually decreased the height of w2 to achieve momentum matching and high-efficiency transform between the guided waves and the spoof SPPs waves.

The spoof SPPs waveguide is composed of three parts: (I) the coplanar waveguide (CPW) as a feeding part to match the 50 Ω input impedance, (II) the momentum matching part from the CPW to spoof SPPs waveguide, and (III) the SSPPs waveguide transmission line, as illustrated in Figure 1d. The dimensions of the SSPPs waveguide are l1 = 10 mm, l2 = 45 mm, l3 = 26.5 mm, w1 = 15 mm. The gap between the ground and the inner metallic strip is set to s = 0.16 mm, which is convenient to connect with 50 Ω Sub-miniature A (SMA) connectors. To achieve the momentum matching, six gradual increases in the height of the units are introduced into our design, with the step of 0.5 mm in the conversion part. We used the time domain solver of the CST Microwave Studio to validate our design and the results are illustrated in Figure 1c. It is clear that a high-efficiency spoof SPPs waveguide is constructed, where the transmission coefficient of the device is around −2 dB and the reflection coefficient is less than −10 dB from 6 GHz to 11 GHz.

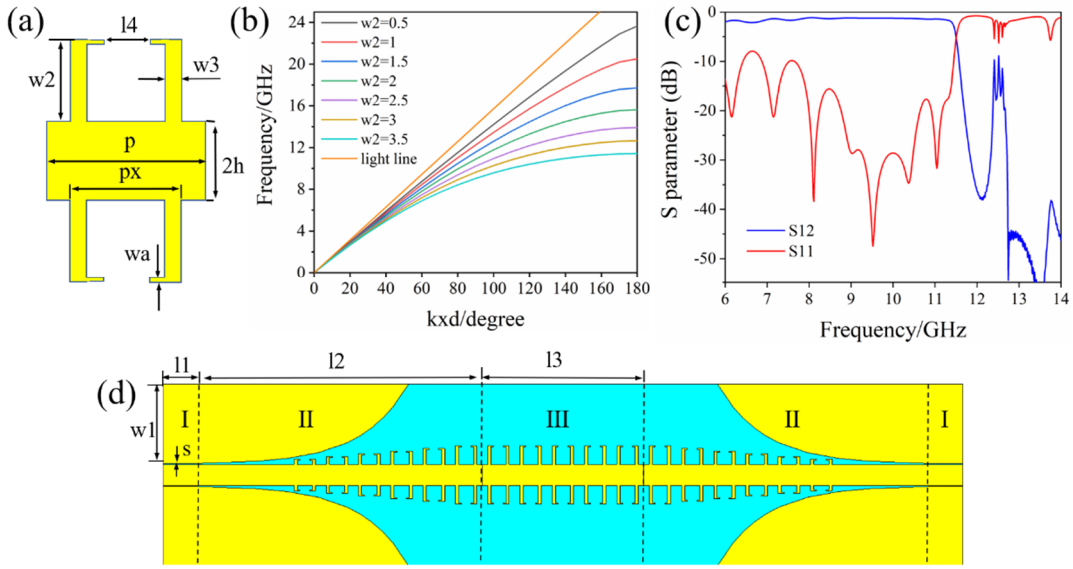

Figure 1. (**a**) The unit structure of the waveguide, whose dimensions are p = 5.3 mm, h = 2 mm, wa = 0.2 mm, px = 3.5 mm, w2 = 3.5 mm, w3 = 0.5 mm, l4 = 1.6 mm. (**b**) Dispersion relations of SSPPs waveguide with different heights. (**c**) The S parameter of the waveguide. (**d**) The schematic diagram of SSPPs waveguide, where l1 = 10 mm, l2 = 45 mm, l3 = 26.5 mm, w1 = 15 mm, s = 0.16 mm.

3. Dynamic Modulation Filter Design and Study

To achieve the dynamic modulation of the transmission and the rejection band, we combine the U-shape and waveguide unit to construct the active unit cell, as shown in Figure 2a. The varactor diodes are loaded at a central position between the U-shape and the waveguide, and we design a through-hole on the U-shape to connect the bottom side metallic strip structure in order to load direct current voltage in the experiment with a top structure. This design enables the dynamic modulation function via changing the capacitance loaded between the U-shape and the waveguide unit.

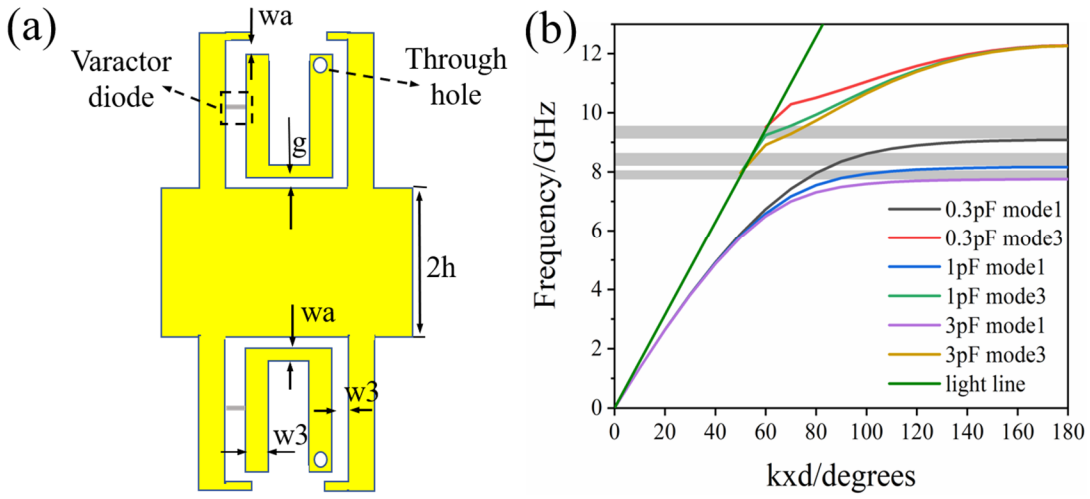

Figure 2. (**a**) The configuration of the dynamic modulation unit cell, where g = 0.2 mm, wa = 0.2 mm, w3 = 0.5 mm. (**b**) Dispersion diagrams of the proposed unit cell at different capacitances.

We can modulate the cut-off frequency of the unit cell by changing the capacitance, while maintaining the same structure and parameter. Figure 2b illustrates the dispersion curves of the proposed active unit cell with regard to different modes and capacitances, which is conducted by the Eigenmode solver in the commercial software CST. We can observe that the dispersion curves deviate from the light line and different modes arrive at different cutoff frequencies, under the same capacitance. From Figure 2b, we found that the cut-off frequency of mode 1 increases along with the decreasing in capacitances. There is a forbidden band between mode 1 and mode 3 under the same capacitance, whose variates correspond to the alteration of the capacitance from about 7.8 GHz to 9.8 GHz. All of this indicates that the configuration can be used to build a dynamic modulation band rejection filter via changing the capacitance. Moreover, in such a symmetrical CPW feeding system, only even mode can be excited, odd mode 2 cannot be excited since the electric field line is asymmetric with respect to the propagation direction.

Based on the above analysis, an active modulation band rejection filter based on spoof SPPs waveguide was realized via changing the capacitance between the U shape and waveguide unit and the configuration of design, as shown in Figure 3. On the bottom side, we designed a metallic strip to connect the direct current voltage via the through-hole in the experiment and used the inductor with 30 μH to connect each independent structure.

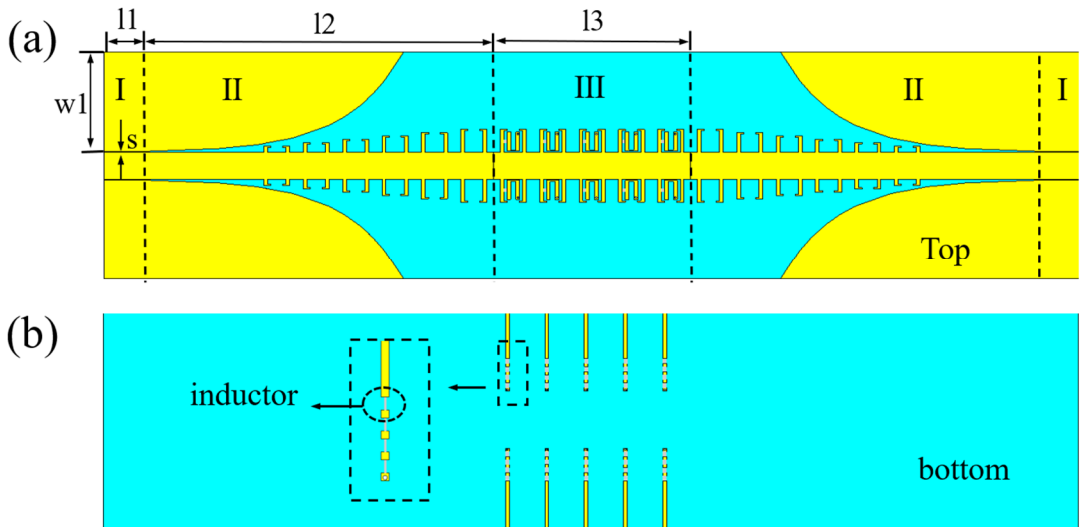

Figure 3. The schematic of the proposed SSPPs dynamic modulation filter. (**a**) The top view. (**b**) The bottom view.

To investigate the transmission performance, we calculated the S-parameter of dynamic modulation spoof SPPs filter with different capacitances and the corresponding results are shown in Figure 4. The transmission coefficients (S12) proves that around a 2 GHz bandwidth band rejection spoof SPPs filter can be achieved and the forbidden band can be accurately controlled by designing the corresponding capacitance.

The transmission coefficients of the filter are around −2 dB under different capacitances in the pass band, meanwhile, in the forbidden band the coefficients can achieve below −35 dB. As depicted in Figure 4, with increasing the capacitance, the forbidden band will shift to a lower frequency. When capacitances are set to 0.3 pF, 1 pF, 3 pF, the forbidden bands (transmission coefficients below −10 dB) are 7.8–8.3 GHz, 8.2–8.7 GHz, 9.2–9.7 GHz, respectively, which coincide with the dispersion curve shown in Figure 2b.

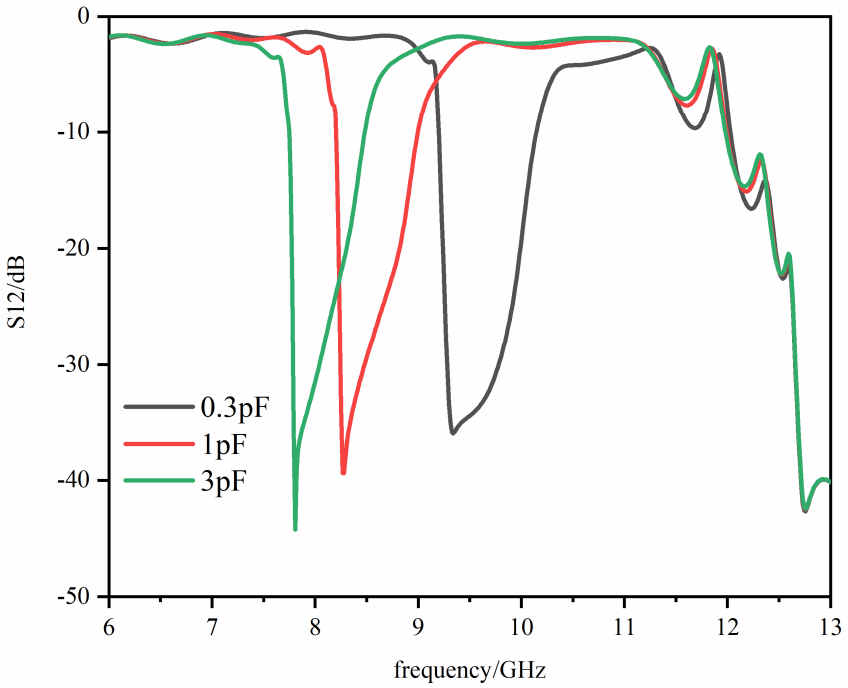

Figure 4. The simulation results of transmission coefficients under capacitances of 0.3 pF, 1 pF and 3 pF.

To have a visual impression for the filter, we simulated the near-electric field distribution. We selected three different rejection frequencies at different capacitances and one pass band frequency. Figure 5 demonstrates the results of near-electric field distribution at 7.8 GHz, 8.3 GHz, 9.5 GHz, 11 GHz with capacitances of 3 pF, 1 pF, 0.3 pF, respectively. It can be seen from Figure 5a–c that the electromagnetic wave is reflected and cannot propagate from one port to another port when the frequency is located at the forbidden band.

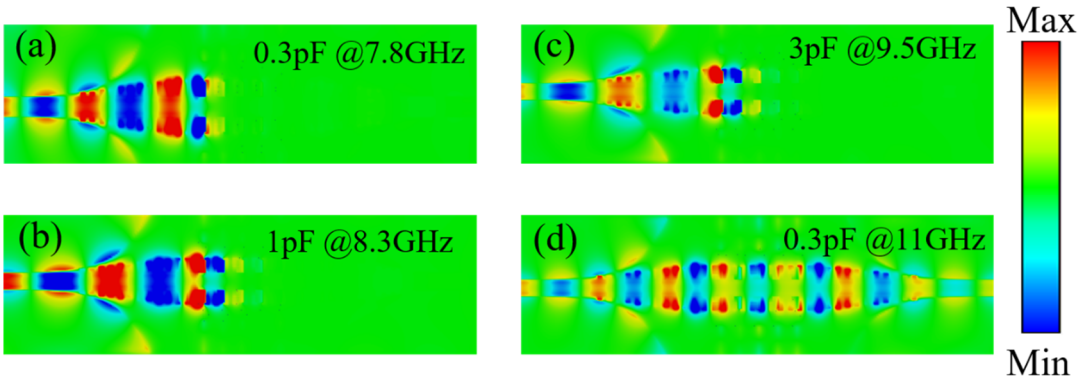

Figure 5. The simulated near-field distribution of the device at (**a**) 7.8 GHz with capacitance 3 pF, (**b**) 8.3 GHz with capacitance 1 pF, (**c**) 9.5 GHz with capacitance 0.3 pF, (**d**) 11 GHz with capacitance 0.3 pF.

The electromagnetic wave can be efficiently transmitted at the same capacitance when the frequency located pass band is between the forbidden band and the cutoff frequency of mode 3, as shown in Figure 5d. From the near-field electric distribution, we can observe that the filter has a better cut-off function at the rejection band and passes the other frequencies efficiently, while keeping the highly field confined.

4. Fabrication and Measurement

To demonstrate the performance of the proposed filter, we fabricated the sample based on the standard printed circuit board process, as shown in Figure 6a. We used SMA and coaxial cables, whose insertion loss is less than about 1 dB, to connect the sample and the vector network analyzer (VNA). In the experiment, we used varactor-diodes (SMV2202-040LF), which were purchased from Skyworks, to realize the dynamic modulation function.

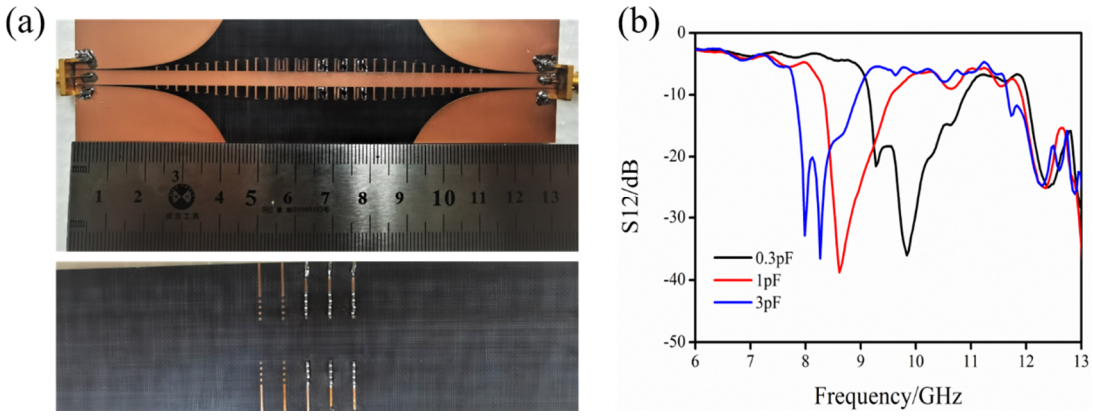

Figure 6. (**a**)The picture of fabricated sample (**b**) Measured S-parameter under different capacitances.

The measured S-parameter results with different bias voltages loaded on the varactor diodes are displayed in Figure 6b. We selected three different loading bias voltages, 0 V, 7 V, 20 V, and the corresponding capacitances are 3 pF, 1 pF, 0.3 pF, to measure the transmission coefficients S12. The position of the rejection band changes from 7.8 GHz to 9.9 GHz, along with the variation of voltage loaded on the varactors. From Figure 6b, we can clearly observe that there are three band rejection bands with isolation values below −30 dB, that maintain a high transmission efficiency in the pass band. Namely, the measured S12 results have a good agreement with the simulations, as listed in Figure 2b. We used the homemade near-field mapper to plot the near electric distribution above the substrate plane at 1 mm. From obtained results displayed in Figure 7a–d, we clearly found that the surface electromagnetic wave is rejected at the forbidden band frequencies 7.8 GHz, 8.3 GHz, 9.5 GHz, corresponding to different capacitances. Furthermore, the electromagnetic wave can propagate along the device in the pass band 11 GHz, which coincides with simulated results.

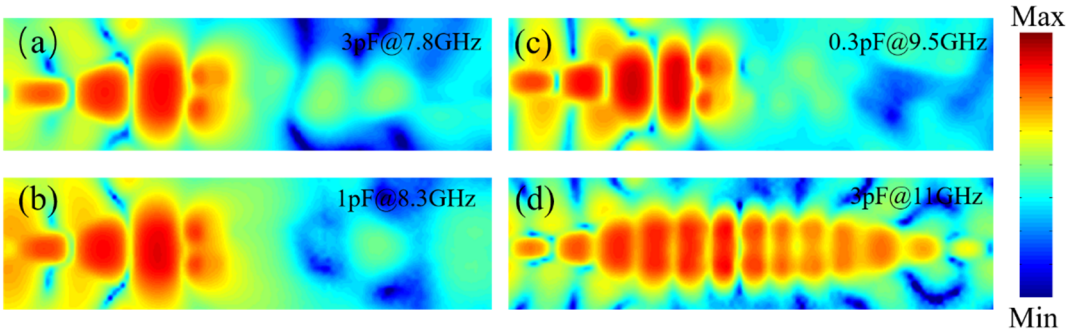

Figure 7. The measured near-field distribution of the device at (**a**) 7.8 GHz with capacitance 3 pF, (**b**) 8.3 GHz with capacitance 1 pF, (**c**) 9.5 GHz with capacitance 0.3 pF, (**d**) 11 GHz with capacitance 0.3 pF.

There are some discrepancies between simulations and measurements which may be caused by insertion loss, inhomogeneity of the substrate, loss of coaxial cables and SMA. Moreover, the shift of frequency between simulation and experiment would be caused by machine error and the imprecise voltage loaded on the varactors.

5. Conclusions

In this paper, a simpler method to fabricate a dynamic modulation band rejection filter device loaded with varactor-diodes has been proposed and manufactured. Based on this method, we can modulate the rejection band in real time, at high speed, by changing the bias voltage. Both the simulation and measurement results have demonstrated a good performance of the filter in tuning the rejection of spoof SPPs, which provides high isolation in the rejection band and maintains high efficiency transmission at the passband. The simpler configuration makes our dynamic modulation filter more compact and gives a method for future dynamic modulation device. By designing the bias voltage loaded on capacitance, it is expected that the proposed method will achieve other multiple function devices such as a logic gate device and a multiple-band rejection filter. The proposed method and structure may pave a new way for the application of SSPPs-based devices and integrated circuit systems in the microwave and THz frequencies.

Author Contributions: X.S. and Y.L. methodology; W.Y. and L.L. design; W.Y. and L.L. writing; Z.L. and L.D. review. All authors have read and agreed to the published version of the manuscript.

Funding: This work is supported by the National Natural Science Foundation of China (NSFC) under Grant 11504210, and the Shanxi Provincial Foundation for Returned Scholars, China (Grant No.2015-096).

Conflicts of Interest: The authors declare no conflict of interest.

References

1. Barnes, W.L.; Dereux, A.; Ebbesen, T.W. Surface plasmon subwavelength optics. *Nature* **2003**, *424*, 824–830. [CrossRef] [PubMed]
2. Foley, J.J.; McMahon, J.M.; Schatz, G.C.; Harutyunyan, H.; Wiederrecht, G.P.; Gray, S.K. Inhomogeneous Surface Plasmon Polaritons. *ACS Photonics* **2014**, *1*, 739–745. [CrossRef]
3. Xu, X.G.; Ghamsari, B.G.; Jiang, J.H.; Gilburd, L.; Andreev, G.O.; Zhi, C.; Bando, Y.; Golberg, D.; Berini, P.; Walker, G.C. One-dimensional surface phonon polaritons in boron nitride nanotubes. *Nat. Commun.* **2014**, *5*, 4782. [CrossRef] [PubMed]
4. Fang, N.; Lee, H.; Sun, C.; Zhang, X. Sub-diffraction-limited optical imaging with a silver superlens. *Science* **2005**, *308*, 534–537. [CrossRef]
5. Yin, L.; Vlasko-Vlasov, V.K.; Pearson, J.; Hiller, J.M.; Hua, J.; Welp, U.; Brown, D.E.; Kimball, C.W. Subwavelength Focusing and Guiding of Surface Plasmons. *Nano Lett.* **2005**, *5*, 1399–1402. [CrossRef]
6. Moreno, E.; Rodrigo, S.G.; Bozhevolnyi, S.I.; Martin-Moreno, L.; Garcia-Vidal, F.J. Guiding and focusing of electromagnetic fields with wedge plasmon polaritons. *Phys. Rev. Lett.* **2008**, *100*, 023901. [CrossRef]
7. Wiecha, M.M.; Al-Daffaie, S.; Bogdanov, A.; Thomson, M.D.; Yilmazoglu, O.; Kuppers, F.; Soltani, A.; Roskos, H.G. Direct Near-Field Observation of Surface Plasmon Polaritons on Silver Nanowires. *ACS Omega* **2019**, *4*, 21962–21966. [CrossRef]
8. Yanik, A.A.; Huang, M.; Kamohara, O.; Artar, A.; Geisbert, T.W.; Connor, J.H.; Altug, H. An optofluidic nanoplasmonic biosensor for direct detection of live viruses from biological media. *Nano Lett.* **2010**, *10*, 4962–4969. [CrossRef]
9. Zeng, S.; Baillargeat, D.; Ho, H.P.; Yong, K.T. Nanomaterials enhanced surface plasmon resonance for biological and chemical sensing applications. *Chem. Soc. Rev.* **2014**, *43*, 3426–3452. [CrossRef]
10. Huang, T.; Zeng, S.; Zhao, X.; Cheng, Z.; Shum, P. Fano Resonance Enhanced Surface Plasmon Resonance Sensors Operating in Near-Infrared. *Photonics* **2018**, *5*, 23. [CrossRef]
11. Jiang, L.; Zeng, S.; Xu, Z.; Ouyang, Q.; Zhang, D.H.; Chong, P.H.J.; Coquet, P.; He, S.; Yong, K.T. Multifunctional Hyperbolic Nanogroove Metasurface for Submolecular Detection. *Small* **2017**, *13*, 1700600. [CrossRef] [PubMed]

12. de Hoogh, A.; Opheij, A.; Wulf, M.; Rotenberg, N.; Kuipers, L. Harmonics Generation by Surface Plasmon Polaritons on Single Nanowires. *ACS Photonics* **2016**, *3*, 1446–1452. [CrossRef] [PubMed]
13. Li, Y.; Kang, M.; Shi, J.; Wu, K.; Zhang, S.; Xu, H. Transversely Divergent Second Harmonic Generation by Surface Plasmon Polaritons on Single Metallic Nanowires. *Nano Lett.* **2017**, *17*, 7803–7808. [CrossRef]
14. Ozbay, E. Plasmonics: Merging photonics and electronics at nanoscale dimensions. *Science* **2006**, *311*, 189–193. [CrossRef] [PubMed]
15. Zhang, H.C.; Liu, S.; Shen, X.; Chen, L.H.; Li, L.; Cui, T.J. Broadband amplification of spoof surface plasmon polaritons at microwave frequencies. *Laser Photonics Rev.* **2015**, *9*, 83–90. [CrossRef]
16. Williams, C.R.; Andrews, S.R.; Maier, S.A.; Fernández-Domínguez, A.I.; Martín-Moreno, L.; García-Vidal, F.J. Highly confined guiding of terahertz surface plasmon polaritons on structured metal surfaces. *Nat. Photonics* **2008**, *2*, 175–179. [CrossRef]
17. Huang, Y.; Fang, Y.; Zhang, Z.; Zhu, L.; Sun, M. Nanowire-supported plasmonic waveguide for remote excitation of surface-enhanced Raman scattering. *Light Sci. Appl.* **2014**, *3*, e199. [CrossRef]
18. Pendry, J.B.; Martin-Moreno, L.; Garcia-Vidal, F.J. Mimicking surface plasmons with structured surfaces. *Science* **2004**, *305*, 847–848. [CrossRef]
19. Hibbins, A.P.; Evans, B.R.; Sambles, J.R. Experimental verification of designer surface plasmons. *Science* **2005**, *308*, 670–672. [CrossRef]
20. Fernández-Domínguez, A.I.; Moreno, E.; Martín-Moreno, L.; García-Vidal, F.J.J.O.L. Terahertz wedge plasmon polaritons. *Opt. Lett.* **2009**, *34*, 2063–2065. [CrossRef]
21. Ma, H.F.; Shen, X.; Cheng, Q.; Jiang, W.X.; Cui, T.J. Broadband and high-efficiency conversion from guided waves to spoof surface plasmon polaritons. *Laser Photonics Rev.* **2014**, *8*, 146–151. [CrossRef]
22. Shen, X.; Cui, T.J.; Martin-Cano, D.; Garcia-Vidal, F.J. Conformal surface plasmons propagating on ultrathin and flexible films. *Proc. Natl. Acad. Sci. USA* **2013**, *110*, 40–45. [CrossRef] [PubMed]
23. Tang, W.X.; Zhang, H.C.; Ma, H.F.; Jiang, W.X.; Cui, T.J. Concept, Theory, Design, and Applications of Spoof Surface Plasmon Polaritons at Microwave Frequencies. *Adv. Opt. Mater.* **2019**, *7*, 1800421. [CrossRef]
24. Zhao, L.; Zhang, X.; Wang, J.; Yu, W.; Li, J.; Su, H.; Shen, X. A Novel Broadband Band-pass Filter Based on Spoof Surface Plasmon Polaritons. *Sci. Rep.* **2016**, *6*, 36069. [CrossRef]
25. Liu, L.; Wang, J.; Yin, X.; Chen, Z. Wide-Angle Beam Scanning Leaky-Wave Antenna Using Spoof Surface Plasmon Polaritons Structure. *Electronics* **2018**, *7*, 348. [CrossRef]
26. Itami, G.; Sakai, O.; Harada, Y. Two-Dimensional Imaging of Permittivity Distribution by an Activated Meta-Structure with a Functional Scanning Defect. *Electronics* **2019**, *8*, 239. [CrossRef]
27. Wang, M.; Ma, H.F.; Tang, W.X.; Zhang, H.C.; Wang, Z.X.; Cui, T.J. Programmable controls of multiple modes of spoof surface plasmon polaritons to reach reconfigurable plasmonic devices. *Adv. Mater. Technol.* **2019**, *4*, 1800603. [CrossRef]
28. Zhang, H.C.; Cui, T.J.; Xu, J.; Tang, W.; Liu, J.F. Real-time controls of designer surface plasmon polaritons using programmable plasmonic metamaterial. *Adv. Mater. Technol.* **2017**, *2*, 1600202. [CrossRef]
29. Ma, Q.; Cui, T.J. Information Metamaterials: Bridging the physical world and digital world. *PhotoniX* **2020**, *1*, 1. [CrossRef]
30. Zhang, X.; Tang, W.X.; Zhang, H.C.; Xu, J.; Bai, G.D.; Liu, J.F.; Cui, T.J. A Spoof Surface Plasmon Transmission Line Loaded with Varactors and Short-Circuit Stubs and Its Application in Wilkinson Power Dividers. *Adv. Mater. Technol.* **2018**, *3*, 1800046. [CrossRef]
31. Chen, K.; Feng, Y.; Monticone, F.; Zhao, J.; Zhu, B.; Jiang, T.; Zhang, L.; Kim, Y.; Ding, X.; Zhang, S.; et al. A Reconfigurable Active Huygens' Metalens. *Adv. Mater.* **2017**, *29*, 1606422. [CrossRef] [PubMed]
32. Zhu, W.; Song, Q.; Yan, L.; Zhang, W.; Wu, P.C.; Chin, L.K.; Cai, H.; Tsai, D.P.; Shen, Z.X.; Deng, T.W.; et al. A flat lens with tunable phase gradient by using random access reconfigurable metamaterial. *Adv. Mater.* **2015**, *27*, 4739–4743. [CrossRef] [PubMed]
33. Ratni, B.; de Lustrac, A.; Piau, G.-P.; Burokur, S.N. Electronic control of linear-to-circular polarization conversion using a reconfigurable metasurface. *Appl. Phys. Lett.* **2017**, *111*, 214101. [CrossRef]
34. Huang, C.; Zhang, C.; Yang, J.; Sun, B.; Zhao, B.; Luo, X. Reconfigurable metasurface for multifunctional control of electromagnetic waves. *Adv. Opt. Mater.* **2017**, *5*, 1700485. [CrossRef]
35. Wang, Z.X.; Zhang, H.C.; Lu, J.; Xu, P.; Wu, L.W.; Wu, R.Y.; Cui, T.J. Compact filters with adjustable multi-band rejections based on spoof surface plasmon polaritons. *J. Phys. D Appl. Phys.* **2019**, *52*, 025107. [CrossRef]

36. Zhao, S.; Zhang, H.C.; Zhao, J.; Tang, W.X. An ultra-compact rejection filter based on spoof surface plasmon polaritons. *Sci. Rep.* **2017**, *7*, 10576. [CrossRef]
37. Zhou, Y.J.; Xiao, Q.X. Electronically controlled rejections of spoof surface plasmons polaritons. *J. Appl. Phys.* **2017**, *121*, 123109. [CrossRef]
38. Xu, J.; Zhang, H.C.; Tang, W.; Guo, J.; Qian, C.; Li, W. Transmission-spectrum-controllable spoof surface plasmon polaritons using tunable metamaterial particles. *Appl. Phys. Lett.* **2016**, *108*, 191906. [CrossRef]

© 2020 by the authors. Licensee MDPI, Basel, Switzerland. This article is an open access article distributed under the terms and conditions of the Creative Commons Attribution (CC BY) license (http://creativecommons.org/licenses/by/4.0/).